Lateral Resolution of an Infrared Visible Optical Sum Frequency Generation Confocal Microscope

Nguyen Anh Tuan[1,2], Yoshihiro Miyauchi[1,2], and Goro Mizutani[1,2,*]

[1]*School of Materials Science, Japan Advanced Institute of Science and Technology, Nomi, Ishikawa 923-1292, Japan*

[2]*Japan Science and Technology Corporation, Core Research for Evolutional Science and Technology, Chiyoda, Tokyo 102-8666*

[*]*E-mail address: mizutani@jaist.ac.jp*

We have demonstrated experimentally that an infrared visible sum frequency generation (SFG) confocal microscope with an objective lens of numerical aperture 0.45 has a lateral resolution of 0.48±0.06 μm. As samples for the demonstration, we used a ZnS(100) wafer with a structure fabricated by a focused ion beam method and a ZnS polycrystalline pellet. The result was consistent with the theoretical resolution of a confocal microscope.

1. Introduction

Imaging techniques are important in various fields and optical sum frequency generation (SFG) microscopy has been used to monitor molecular vibrational images on surfaces and in biological materials[1-3]. SFG is one of the lowest-order nonlinear optical processes and it occurs in noncentrosymmetric media [4,5]. Other vibrational microscopies, such as infrared and Raman microscopies [6-9] do not have such selectivity for asymmetric species. Here molecular vibrational spectra have a lot of useful information. They provide information on local functional groups and their orientation. The fine structure of the spectral peaks gives information on the higher order structures of polymers and the crystalline order state [3]. Hence, it is important to develop vibrational infrared, Raman, and SFG microscopies in a synchronous and complementary manner to be able to apply them to the development of solid state physics, biology, and their related technologies.

The first SFG microscopy (SFGM) was demonstrated in 1999 by Flörsheimer et al. using a Langmuir-Blodgett film as a sample,[10] and it was followed by other observations of organic-molecular systems [1)3)11-17)] as well as inorganic samples [2)18)-21)]. Cimatu et al. distinguished between different chain-length self-assembled monolayers in microprinted patterns [1]. Nakai et al. observed electric field-induced SFG images of organic field-effect transistors [13]. Miyauchi et al. observed an SFG image of a water plant *Chara fibrosa* and detected amylopectin selectively in it utilizing the sensitivity of this method for chirality [3]. Recently, Inoue and coworkers have reported an SFGM resolution better than 2 μm using an onion root cell as a sample [14,15].

There has also been effort to improve the spatial resolution of SFGM. Infrared visible SFG has been detected by near-field scanning optical microscopy (NSOM) with a spatial resolution of 0.19 μm [11]. There has also been a combination of visible SFG and far-field

confocal microscopy [9]. Examples of SHG confocal micrsocopy show that the confocal optics gives nonlinear optical images with a resolution better than the diffraction limit and facilitates three-dimensional scanning [22,23]. However, a combination of the confocal optics and infrared visible SFGM has not been attempted except for the works by our group below.

Locharoenrat et al proposed the first infrared visible SFG confocal microscope [20]. In their optical setup, they combined a normal confocal microscope (we call this a linear confocal microscope henceforth) with a loosely focused infrared beam irradiating the sample from an off-axis direction. The overlapped volume of the visible and infrared light beams provided the radiation source of SFG. The radiation source was scanned on the sample and the SFG image was obtained. The collection optical path of the signal light for the linear image observation of the 532 nm light was the same as that for the SFG image observation of the 460 nm light. The optical setup was just the same as the Raman microscopy setup in the anti-Stokes mode. Hence, their equipment had an advantage in that the SFG image would be taken with little or no readjustment of the optical path after the linear image was taken.

Images of SFG intensity from ZnS polycrystals were obtained with a spatial resolution of 2 μm [21]. They also demonstrated the acquisition of images of SFG intensity of ZnS polycrystalline planes at different depths [20]. Hieu et al. and Li et al. used the same microscopy and obtained SFG images of cellulose fibers and rice grains, respectively [16,17]. However, in theie observations, the spatial resolution of the confocal SFG microscope was far worse than the minimum theoretical limit of 0.44 μm explained below. In fact, the SFG signal became remarkably weaker as the smaller pinhole was used, and it was difficult to optimize the optical arrangement manually. Thus, those works ended up with only a trial demonstration with a moderate spatial resolution. According to Cox and Sheppard,[24] it is practically difficult to reach

exactly the theoretically optimum spatial resolution of the confocal microscope. This is especially the case of SFG microscopy for bulky samples. In this context, the optimum lateral resolution of the SFG confocal microscope of the type constructed by Locharoenrat et al. is also worth checking experimentally, which becomes the purpose of this study.

As the test sample, we used a single crystal ZnS(100) wafer with a geometrical structure fabricated by focused ion beams. Since the single crystal zincblende ZnS has a macroscopic noncentrosymmetric structure, the infrared and visible beams can couple nonlinearly and will permit an intense SFG from the bulk region of the crystal [4,5]. The polycrystalline ZnS used by Locharoenrat et al. was not useful for the present purpose, because the SFG from it is expected to occur in a random direction and may not hit the objective lens, as we will discuss later. Still, we also measured the SFG images of the polycrystalline ZnS and used them to obtain the spatial resolution.

As discussed by Cox and Sheppard and other groups, the minimum resolved distance r between two points obtained by confocal microscopy is given by [24-27]

$$r = \frac{0.61\lambda}{\sqrt{2}NA}. \quad (1)$$

Here, λ is the wavelength of the observed light signal and NA is the numerical aperture of the collection optics or the objective lens. The full width half maximum (FWHM) resolution is slightly different from that in eq. (1)[24]. Furthermore, the resolution in a coherent light emission case such as SFG, is generally worse than that given by eq. (1)[24]. However, for simplicity, we compare every result in this study with eq. (1), because it is the most popular form of the resolution of confocal microscopy.

When we put λ = 460 nm and NA = 0.45 for our confocal SFG microscope into eq. (1), we obtain a resolution of 0.44 μm. This is the theoretical spatial resolution when an ideally small

pinhole is used. In the present case, 1 Airy unit, or the diameter of the Airy disk [28] at the pinhole, is calculated to be m X 0.61 λ_{exc}/NA =14.4 μm with the magnification factor of the optics m=20. A pinhole in front of the photomultiplier tube with a diameter smaller than 1 Airy unit should give a nearly ideal resolution of the confocal optics. The ideal axial resolution of the confocal microscope is given by [29]

$$Z = \frac{1.41 n \lambda}{NA^2} \quad (2)$$

Here, n is the refractive index of the medium. When we put the refractive index n_{ZnS} = 2.29 at λ = 460 nm and NA =0.45 into eq. (2), we obtain Z = 7.3 μm.

2. Experimental Procedure

Figure 1 shows the optical setup of our sum frequency generation confocal microscopy system. It is basically the same as our previous optical setup [20]. The source of the visible light at λ_{VIS} = 532 nm was the doubled-frequency output from a mode-locked neodymium-doped yttrium aluminum garnet (Nd:YAG) laser (EKSPLA PL2143B). The light pulses of 532 nm wavelength with the pulse duration time of 30 ps and at the repetition rate of 10 Hz entered the commercial microscope optics Nikon Eclipse LV100D along its optical axis. The tunable infrared light from an optical parametric generator and amplifier system (EKSPLA PG501/DFG) driven by the fundamental and second harmonic outputs of the same Nd:YAG laser were focused on the same position as the 532 nm light on the sample by a CaF_2 lens of 250 mm focal length. The infrared light source with a bandwidth of 6 cm^{-1} was chosen in order to have a good vibrational spectrum, sacrificing the measurement speed due to the low repetition rate [30]. The pulse energies of the visible and infrared beams at the sample surface were 10 and 5 μJ/pulse, respectively. The

visible and infrared beams were incident on the sample with incident angles of 0 and 62^{o}, respectively. The angle of 62^{o} was chosen so that the infrared beam was not blocked by the objective lens before it illuminates the sample. The spot size of the infrared light was around 30 μm on the sample. The SFG light pulses that travelled back on the optical path of the incident visible light as shown by dashed lines in Fig. 1 were reflected by a dichroic mirror (DCM), focused on the pinhole, and detected by a photomultiplier. The SFG intensity was measured at an infrared wave number of around 2890 cm^{-1} (λ_{IR} ~ 3 μm). This infrared wave number was chosen because it was frequently used in our past analyses of the CH vibrational region of hydrocarbons [3,16,17]. When the infrared wave number was scanned between 2750 and 3150 cm^{-1}, the beam spot shifted by 300 μm at maximum on the sample plane owing to the change of the oscillation condition in the OPG. Thus, the readjustment of the infrared beam was necessary in order to obtain images at different wave numbers. The SFG signal appeared at λ_{SFG} ~ 460 nm.

Figure 2 shows the details of the optical elements used in the visible incident and collection optics. As a DCM, we used a single-edge dichroic beamsplitter with a nominal edge wavelength of 506 nm (Semrock FF506). The beamsplitter passed the 532 nm light pulses but reflected the 460 nm SFG pulses. The focal lengths of the lenses were chosen so that the beam sizes at the mirrors in the optical paths do not exceed 15 mm. The lenses L23, L24, L25, and L30 were visible achromatic doublets. L23 and L30 were Thorlabs AC254-100-A1 (f=100 mm), and L24 and L25 were Thorlabs AC254-400-A1 (f=400 mm). The objective lens was Nikon LUPlan Fluor 20X/0.45NA and was mounted on z-axis piezo-stage Nano-servo NS7111-C with the travel range of 100 μm. The band pass filters in front of the photomultiplier (Hamamatsu R-585S) were Thorlabs FB460-10 (FWHM bandwidth, 10 nm) for a 460 nm wavelength and Semrock FF01-472/30-25 (FWHM bandwidth, 30 nm) for a 472 nm wavelength. The x-y piezo-

stage and the controller were NANO CONTROL NS4213 and NC3301-C, respectively. The travel range of this piezo-stage was 100 x 100 μm^2. The pinhole of 10 μm diameter corresponding to 0.69 Airy units was Thorlabs P10S. The spatial resolutions should be ~110% of those predicted from Eq. (1) [24]. The image at the sample was magnified 20 times at the pinhole. SFG intensities were normalized by the intensity of the incident infrared light. A linear image with an area of 400 x 400 μm^2 was also monitored by a charge-coupled device (CCD) camera (Trinity IUC-130CN2), in addition to linear confocal microscopy images. All SFG experiments were performed in air at room temperature of 24^oC.

In order to evaluate the spatial resolution of the SFG confocal microscopy, we used a ZnS(100) single crystal wafer with a structure fabricated by a Ga focused ion beam. We purchased a ZnS(100) wafer of 10 x 10 x 1 mm^3 size grown by a chemical vapor transport method in hydrogen from RMT Ltd. The focused ion beam (FIB) system SII Technology SMI 3050 with a gallium ion source was used to fabricate the pattern. A beam current of 2 μA and an acceleration voltage of 30 keV energy were used. The desired pattern was milled by rastering the ion beam. The vertical cross-sectional fabrication design is shown in Fig. 3(a). The real fabrication considered an effect of the three dimensional shape of the focused ion beam waist, and the fabricated edges are inferred to exhibit some roundness. In order to avoid charge up of the wafer, the substrate was coated with 10 to 20 nm amorphous carbon and 20 nm PtPd before fabrication. After the ion beam fabrication, this coating was mostly removed by the Ga ion beam. However, part of it remained as was confirmed by optical microscopy observation. SFG was not observed from the area with this residual coating.

The polycrystalline ZnS pellet grown by chemical vapor deposition (CVD) with a diameter of 10 nm and a thickness of 3 mm was purchased from Furuuchi Chemical Co., Ltd., Japan, and it was used as delivered for both linear and SFG image observations.

3. Results and Discussion

First, we evaluated the spatial resolution of the optical microscopy system as a linear confocal microscope using only the 532 nm laser light and the pinhole of 10 μm diameter. We used a ZnS polycrystalline pellet as a sample. Using small pits and scratches on the surface of the ZnS pellet, the lateral resolution was evaluated as 0.49 μm. This is consistent with 110% that of the theoretical prediction of r=0.51 μm obtained from eq. (1). In a similar way, the axial spatial resolution in the depth direction was experimentally evaluated as 5.5 μm. This value is considered to be roughly consistent with 7.3 μm predicted from eq. (2).

Figure 3(b) shows a linear confocal image of the fabricated structure on ZnS(100) by using the 532 nm light only. The horizontal positions of Figs. 3(a)-3(d) are adjusted to each other. In Figs. 3(b) and 3(c), the collection optics are focused on the middle terrace of the fabricated structure. In Fig. 3(b), the circumference of the middle terrace is dark because parts of the incident and reflected light are blocked by the vertical walls surrounding the middle terrace. The top substrate face of the structure is out of focus, but it is almost within the focal depth of 7.3 μm calculated from eq. (2) from the focal plane and is less clear around the middle terrace.

Figure 3(c) shows an SFG confocal image of the sample in the same optical configuration as that in Fig. 3(b). The infrared excitation light irradiated the sample from the right-hand side as shown schematically in Fig. 3(a). The visible excitation light irradiated the sample from its

normal direction. The SFG light propagating upward was collected by the objective lens. The incident angle of the infrared light was as large as 62^{o}; thus, it could not hit all the faces of the sample. The accumulation time of the SFG images in this study 2 h, but we see a very weak image in Fig. 3(c) due to the small pinhole in front of the detection photomultiplier. One may see in Fig. 3(a) that, concerning the middle terrace, the infrared light can irradiate only the left part. Accordingly, in Fig. 3(c), we see weak signals from the left part of the middle terrace, as indicated by a white arrow.

We also see a stronger SFG emitting area to the left of the middle terrace. This area corresponds to an edge structure marked A in Fig. 3(a). Here, SFG is suggested to be strong for two reasons. One reason is that amorphous carbon and Pt-Pd coating on the substrate top is removed by the tail of the focused ion beam and the bare ZnS crystal was exposed. Hence this area can emit a strong SFG. Another possible reason is that the fabricated edge A is slightly dull owing to the nonideal FIB fabrication at the beam waist. The infrared beam with the incident angle of 62^{o} may hit the substrate more effectively at point A when the edge is round than when it is sharp, since a wider ZnS surface should be exposed to the infrared beam with a lower incident angle.

We evaluated the spatial resolution of the SFG microscope using this stronger signal near edge A. We adjusted the focus of our system to the top face of the sample and obtained the SFG image in Fig. 3(d). In Fig. 3(d), the signal from the middle terrace is weaker, and the image of the strong SFG signal is narrower than that in Fig. 3(c). In Fig. 4, we show the SFG intensity profile along the horizontal line in Fig. 3(d). Fitting the profile to the error function, we estimated the resolution as 0.53 μm.

In order to collect additional data for evaluating the spatial resolution of the confocal SFGM, we used a polycrystalline ZnS pellet as a sample. Figures 5(b)-5(d) show its SFG intensity images, while Fig. 5(a) shows the corresponding linear CCD image. In Figs. 5(b)-5(d), SFG occurs in very small spots on the sample. We also found that some regions showed SFG images with fine structures. These fine structures are due to geometrical structures, such as pits, scratches, or domain boundaries, on the pellet surface.

Using the SFG intensity profiles at two selected positions on the fabricated ZnS(100) substrate and at two selected positions on a polycrystalline ZnS pellet, we evaluated the spatial resolution. From Fig. 4, we obtained a resolution of 0.53 μm and, from another SFG profile at the middle terrace edge in Fig. 3(c), we obtained a resolution of 0.55 μm. Figure 6 shows the SFG intensity profile on the ZnS polycrystalline pellet along the straight line shown in Fig. 5(c). By fitting the error function to the data points in Fig. 6, we obtained a resolution of 0.42 μm. On another point on the ZnS polycrystalline pellet, we obtained a resolution of 0.41 μm. From these four resolutions, the statistically evaluated spatial resolution of the current SFGM was 0.48±0.06 μm. This result is consistent with the lateral resolution of 0.49 μm predicted from eq. (1) multiplied by 1.1. SFG is a coherent process and the ideal spatial resolution of the SFG confocal microscope should be worse than the value predicted from eq. (1) owing to the interference in signal light[24]. However, this difference cannot be discussed in this study owing to the experimental error of ±0.06 μm.

In contrast, we could not evaluate the axial resolution of this microscope in the depth direction. This is because in our depth scan, we only moved the objective lens in the z-direction and did not move the infrared light. Accordingly, the focused visible beam moved in the z-direction but the loosely focused infrared beam did not. Thus, the overlapping of the visible and

infrared beams became worse as the objective lens was scanned in the z-direction. Hence, an accurate depth resolution could not be obtained. Still, we obtained an apparent depth resolution of 1.5 μm. This resolution is better than that obtained from the theoretical prediction of eq. (2), but it is not a true axial resolution for the reason above.

It would be interesting to infer why the polycrystalline ZnS pellet showed weak signals from almost the entire sample area and only spotty SFG images with sizes of around 1 μm, such as those seen in Fig. 5. SFG is a coherent process, and the phase matching among the incident and SFG beams must be optimum for the SFG light to be emitted strongly [4]. Normally, the direction of the optimum phase-matched wave vector is in a narrow solid angle and the SFG light is emitted in a beam. Assuming that the strong beam is oriented in a random direction from each crystalline domain, the probability of this beam to enter the acceptance angle of the objective lens is

$$P = \frac{\Delta\Omega}{4\pi} . \qquad (3)$$

Here, $\Delta\Omega$ is the solid angle of the SFG light in ZnS reaching the objective lens. $\Delta\Omega$ is calculated to be 0.12 sr from the numerical aperture of 0.45 of the objective lens and the refractive index of 2.29 of ZnS at the wavelength of 460 nm. Using eq. (3), we can estimate P as approximately 1%. On the other hand, the area percentage of the strong SFG in the image in Fig. 5 is approximately 0.6%. The rough agreement of these two values can be explained if we assume that the SFG light is generated in a strong beam from bulk ZnS grains with sizes of ~ 1 μm. This SFG source size is probably the single crystal domain size in the polycrystalline matrix. In the linear image of the polycrystalline pellet in Fig. 5(a), we see that the pits created by polishing have a size of

around 1 μm. We infer that the crystalline particle has this size and is dislocated from the matrix during polishing.

In the introduction, we noted that this polycrystalline ZnS pellet was not suitable for the test observation of the SFG confocal microscope with a pinhole size of 10 μm. This was not the case for the lower resolution in ref. 20. This is because the SFG source from a wider and deeper region was within the acceptable range of the objective lens and the larger solid angle from each SFG source was acceptable, for lower resolutions or larger pinholes. However, when we made the pinhole smaller, the signal weakened rapidly at most of the points on the sample, as seen in Fig. 5(b), and we could not optimize the optical setup easily. This was the reason why the polycrystalline ZnS was not simply appropriate as the first test sample for the demonstration of the optimum spatial resolution.

4. Conclusions

We have constructed a confocal sum frequency generation (SFG) microscope and measured its lateral spatial resolution. By observing the SFG images from ZnS(100) fabricated by a focused ion beam method and a polycrystalline ZnS pellet, we obtained the lateral resolution of 0.48±0.06 μm.

Acknowledgment

The authors would like to thank Dr. Takahiro Ode of Nanophoton Corporation for his helpful advice and guidance.

Reference

1) K. Cimatu, H. J. Moore, T. R. Lee, and S. Baldelli: J. Phys. Chem. C **111** (2007) 11751.

2) Y. Miyauchi, H. Sano, J. Okada, H. Yamashita, and G. Mizutani: Surf. Sci. **603** (2009) 2972.

3) Y. Miyauchi, H. Sano, and G. Mizutani: J. Opt. Soc. Am. A **23** (2006) 1687.

4) Y. R. Shen: *The Principles of Nonlinear Optics* (Wiley, New York, 1984) Chap. 2, p. 28 .

5) H. Jayathilake: *Vibrational Sum Frequency Generation Spectroscopy* (VDM Verlag, Saarbrücken, 2010) p.19.

6) A. Boskey and N. P. Camacho: Biomaterials **28** (2007) 2465.

7) P. Yu: J. Struct. Biol. **150** (2005) 81.

8) S. D. Evans, T. L. Freeman, T. M. Flynn, D. N. Batchelder, and A. Ulman: Thin Solid Films **244** (1994) 778.

9) A. Downes, R. Mouras, and A. Elfick: J. Raman Spectrosc. **40** (2009) 757.

10) M. Flörsheimer, C. Brillert, and H. Fuchs: Langmuir **15** (1999) 5437.

11) R. D. Schaller and R. J. Saykally: Langmuir **17** (2001) 2055.

12) G. Mizutani, T. Koyama, S. Tomizawa, and H. Sano: Spectrochim. Acta, Part A **62** (2005) 845.

13) I. F. Nakai, M. Tachioka, A. Ugawa, T. Ueda, K. Watanabe, and Y. Matsumoto: Appl. Phys. Lett. **95** (2009) 243304.

14) K. Inoue, M. Fujii, and M. Sakai: Appl. Spectrosc. **64** (2010) 275.

15) S. Kogure, K. Inoue, T. Ohmori, M. Ishihara, M. Kikuchi, M. Fujii, and M. Sakai: Opt. Express **18** (2010) 13402.

16) H. C. Hieu, N. A. Tuan, H. Li, Y. Miyauchi, and G. Mizutani: J. Appl. Spectrosc. **65** (2011) 1254.

17) H. Li, Y. Miyauchi, N. A. Tuan, G. Mizutani, and M. Koyano: Journal of Biomat. and Nanobiotechnol. **3** (2012) 286.

18) D. M. P. Hoffmann, K. Kuhnke, and K. Kern: Rev. Sci. Instrum. **73** (2002) 3221.

19) K. Kuhnke, D. M. P. Hoffmann, X. C. Wu, A. M. Bittner, and K. Kern: Appl. Phys. Lett. **83** (2003) 3830.

20) K. Locharoenrat, H. Sano, and G. Mizutani: Phys. Status Solidi (C) **6** (2009) 304 [Erratum **6** (2009) 1345].

21) G. Mizutani and Y. Miyauchi: Tech. Dig. OSA Optics Photonics Congr., 2009, paper JWA23/1-3.

22) J. Kaneshiro, S. Kawado, H. Yokota, Y. Uesu, and T. Fukui: J. Appl. Phys. **104** (2008) 054112.

23) T. A. Theodossiou, C. Thrasivoulou, C. Ekwobi, and D. L. Becker: Biophys. J. **91** (2006) 4665.

24) G. Cox and C. J. R. Sheppard: Microsc. Res. Technol. **63** (2004) 18.

25) C. J. R. Sheppard and A. Choudhury: Opt. Acta **24** (1977) 1051.

26) R. H. Webb: Rep. Prog. Phys. **59** (1996) 427.

27) C. J. R Sheppard and M. Gu: Appl. Opt. **30** (1991) 3563.

28) M. Born and E. Wolf: *Principles of Optics* (Cambridge University Press, Cambridge, U. K., 1980) 6^{th} ed., p. 396.

29) K. Carlsson and N. Aslund: Appl. Opt. **26** (1987) 3232.

30) V. Raghunathan, Y. H. O. Korth, N.-H. Ge, and E. O. Potma: Opt. Lett. **36** (2011) 3891.

Figure Captions

Fig. 1. Experimental setup for the measurements of SFG intensity images by optical SFG confocal microscopy. OPG and DFG mean an optical parametric generator and a difference frequency generator, respectively. PMT means a photomultiplier, DCM, a dichroic mirror. CCD camera, a charge-coupled device camera, ND filter, a neutral density filter, and $\lambda/2$, a manually rotatable half-wavelength plate for the 2.33eV light. The visible, infrared, and SFG light pulses travelled on the solid, gray, and dashed lines, respectively. The polarizations of the beams are in the incidence plane of the infrared beam.

Fig. 2. Optical elements used in the visible incident and collection optics. L23, L24, L25, and L30 are achromatic lenses. BPF means a band pass filter, and PH, a pinhole.

Fig. 3. (a) Cross sectional design of the fabricated ZnS(100). The fabricated structure does not appear exactly like this design owing to the nonideal fabrication by FIB. (b) Confocal linear image and (c) confocal SFG image of the fabricated ZnS(100). The focus of the objective lens was adjusted to the middle terrace of the fabricated structure for (b) and (c). (d) Confocal SFG image when the focus of the objective lens was adjusted to the top face. The input visible pulses had a wavelength of 532 nm and the input infrared pulses had a wave number of 2890 cm^{-1}. The accumulation time of the SFG images in (c) and (d) was 2 h.

Fig. 4. SFG intensity profile along the horizontal line drawn in Fig. 3(d). The solid curve represents an error function fitting the experimental data. The display range corresponds to

that indicated by an arrow in the wider profile shown in the inset.

Fig. 5 (a) Visible CCD and (b-d) SFG images of a polycrystalline ZnS pellet. The objective lens was focused at 2μm above, just on, and at 2μm below the pellet surface for (b)-(d), respectively. The input visible pulses had a wavelength of 532nm and the input infrared pulses had a wave number of 2890cm^{-1}. The accumulation time of the SFG images in (b)-(d) was 2 h.

Fig. 6. SFG intensity profile along the horizontal line in Fig. 5(c). The solid curve represents an error function fitting the experimental data. The display range corresponds to that indicated by an arrow in the wider profile shown in the inset.

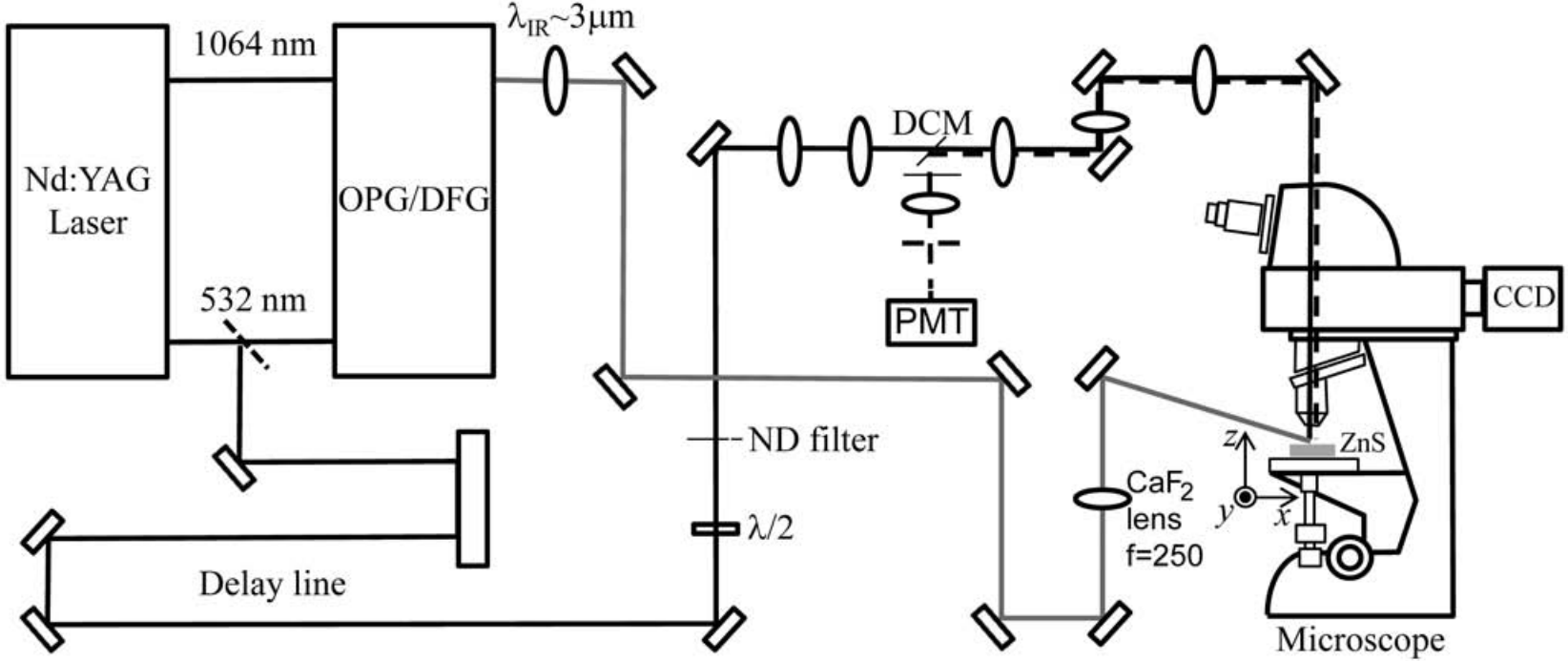
Nd:YAG Laser
1064 nm
532 nm
OPG/DFG
λ_{IR}~3μm
DCM
PMT
CCD
ND filter
λ/2
Delay line
CaF2 lens f=250
ZnS
z
y
x
Microscope

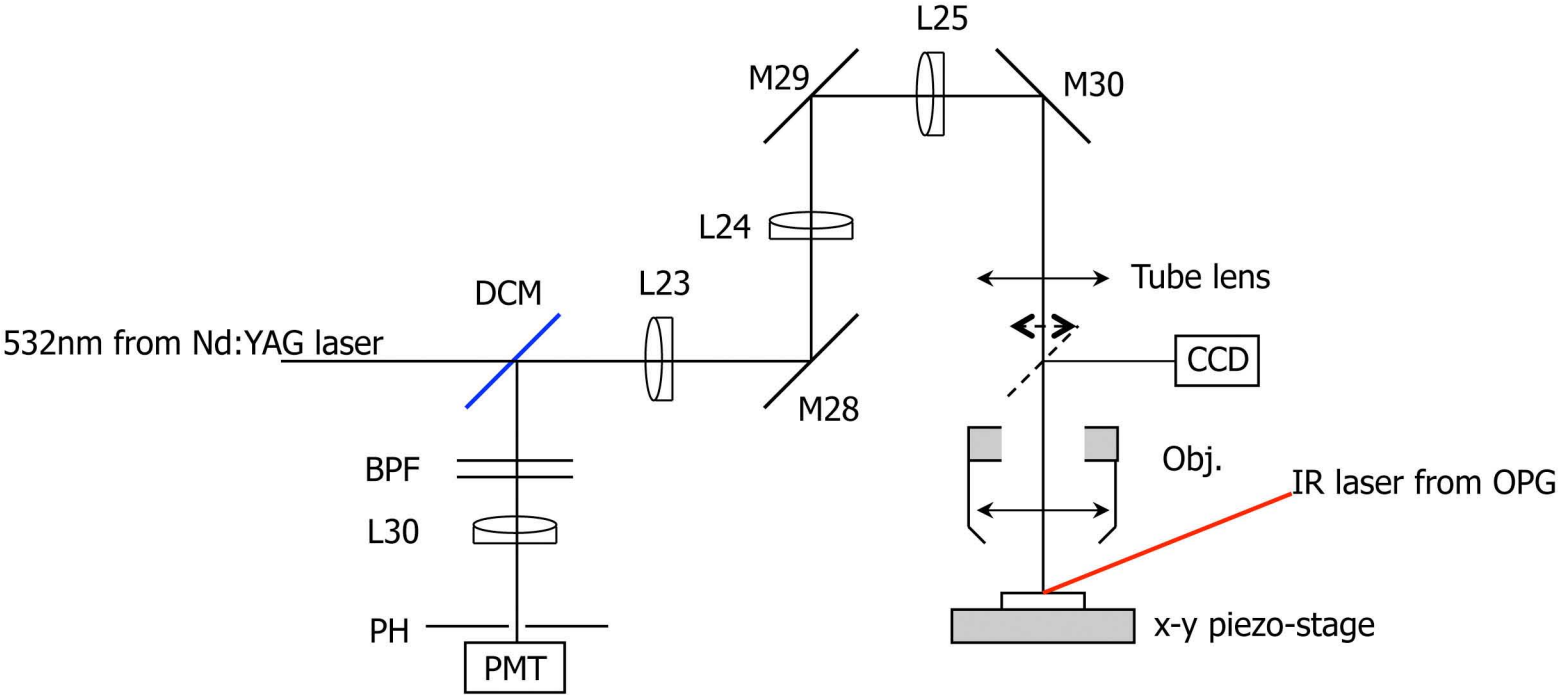
L25
M29
M30
L24
Tube lens
DCM
L23
532nm from Nd:YAG laser
CCD
M28
BPF
Obj.
IR laser from OPG
L30
PH
x-y piezo-stage
PMT

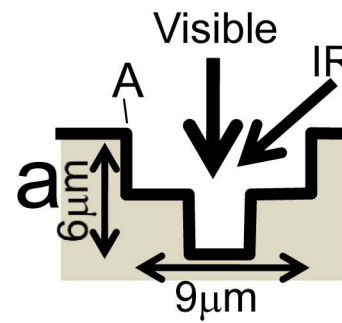
Visible
IR
A
a
9μm
9μm

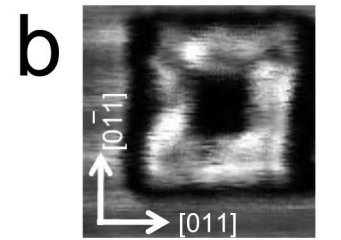
b
[0$\bar{1}$1]
[011]

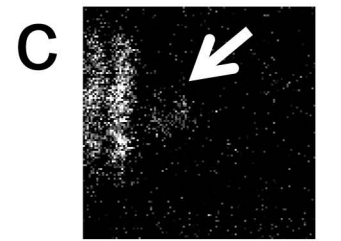
c

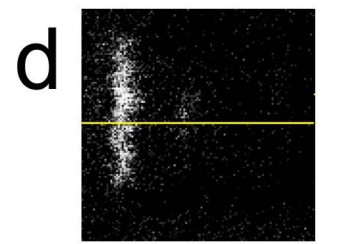
d

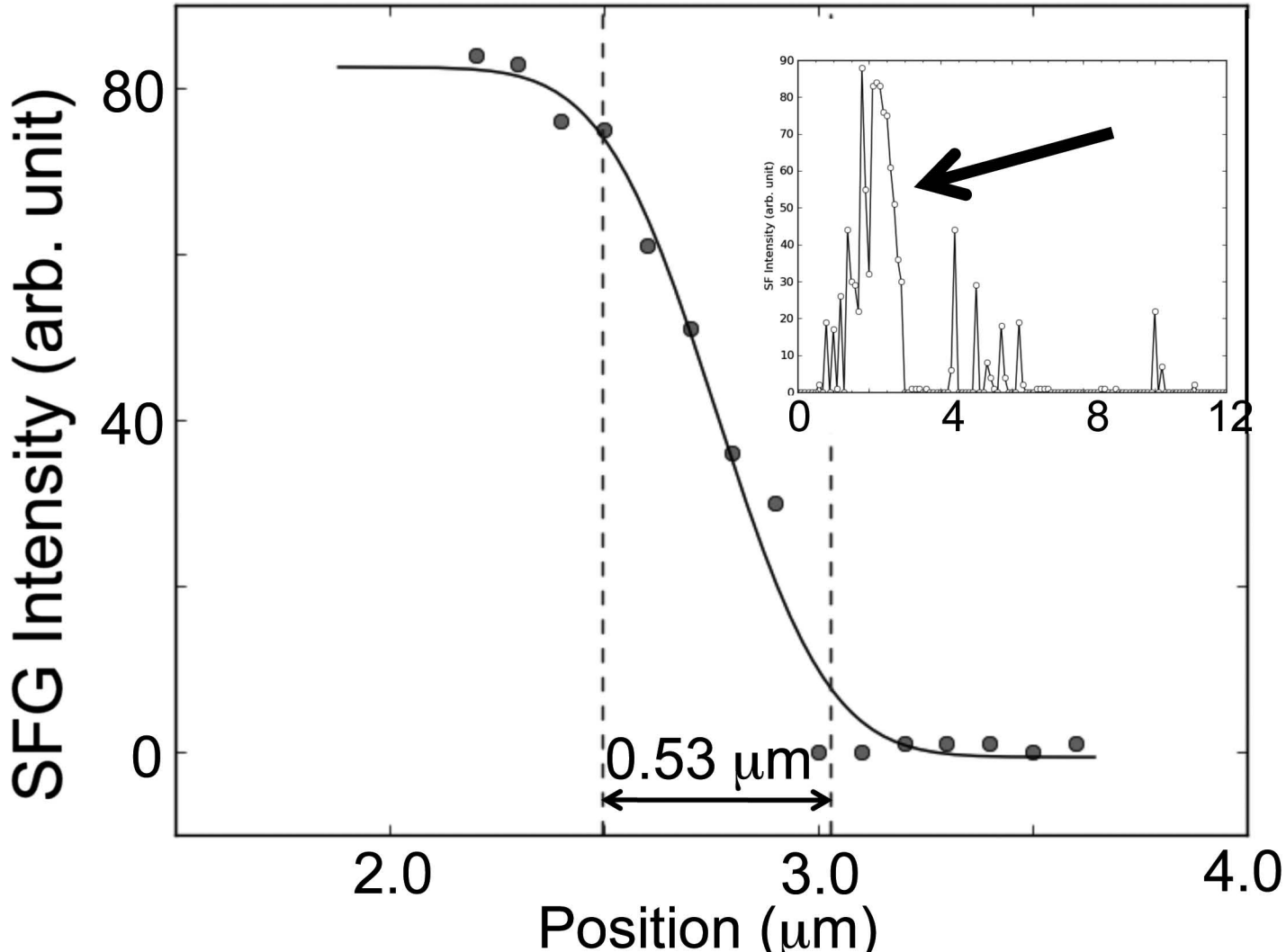
SFG Intensity (arb. unit)
80
40
0
2.0
3.0
4.0
Position (μm)
0.53 μm
SF Intensity (arb. unit)
0
4
8
12

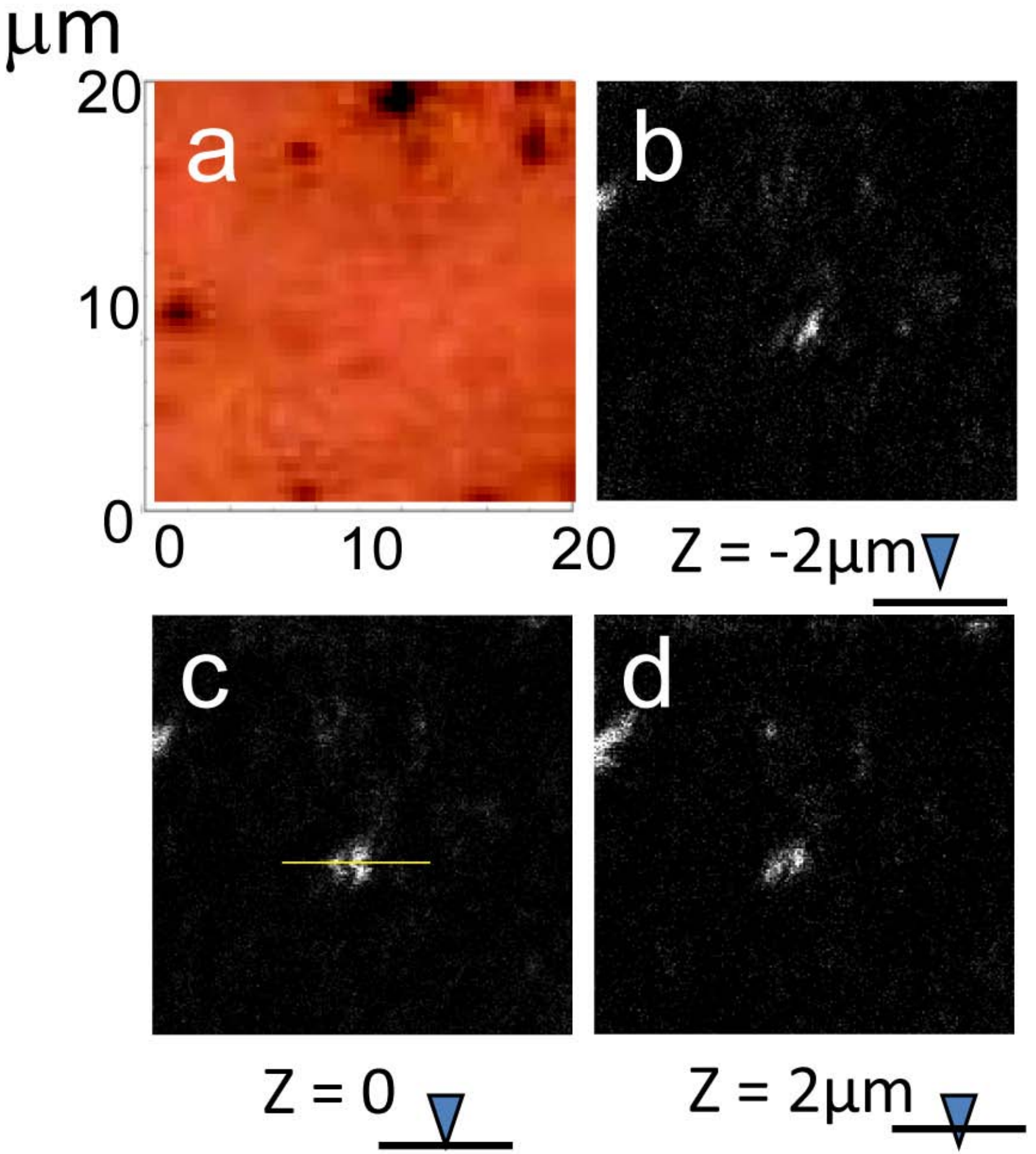
µm
20
10
0
0
10
20
a
b
Z = -2µm
c
d
Z = 0
Z = 2µm

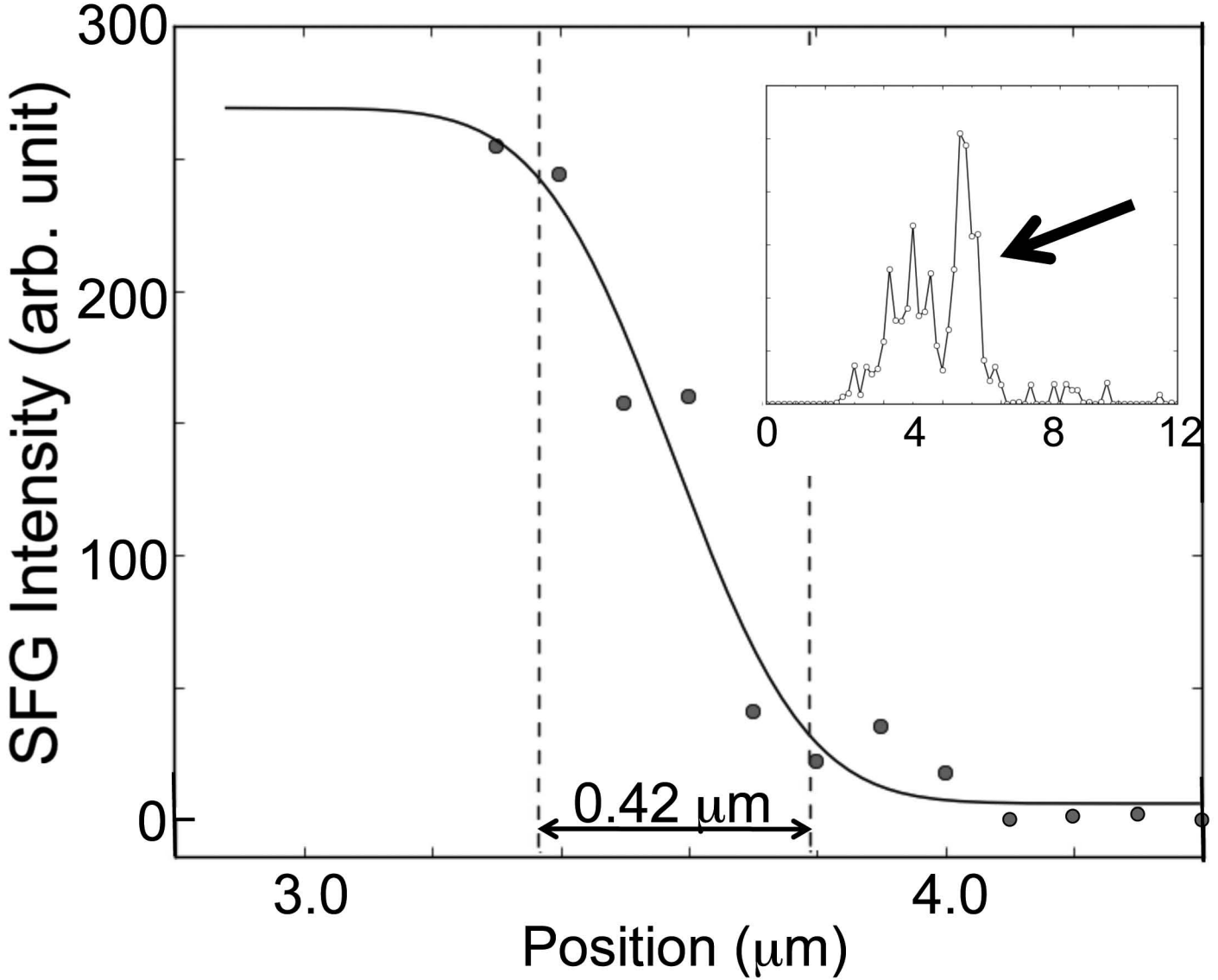
300
200
100
0
SFG Intensity (arb. unit)
3.0
4.0
Position (μm)
0.42 μm
0
4
8
12